Hindawi
Mathematical Problems in Engineering
Volume 2022, Article ID 5029132, 18 pages
https://doi.org/10.1155/2022/5029132

Research Article

A Theoretical Study of Reverse Roll Coating for a Non-Isothermal Third-Grade Fluid under Lubrication Approximation Theory

Fateh Ali,[1] **Muhammad Zahid**,[2] **Yanren Hou**,[1] **Jalil Manafian**,[3,4] **M. A. Rana**,[5] **and Afandiyeva Hajar**[6]

[1]*School of Mathematics & Statistics, Xi'an Jiaotong University, Xi'an, Shaanxi 710049, China*
[2]*Department of Mathematics, COMSATS University Islamabad, Abbottabad Campus, Abbottabad 22060, Pakistan*
[3]*Department of Applied Mathematics, Faculty of Science University of Tabriz, Tabriz, Iran*
[4]*Natural Sciences Faculty, Lankaran State University, 50, H. Aslanov Str., Lankaran, Azerbaijan*
[5]*Department of Mathematics & Statistics, Riphah International University, Sector I-14, Islamabad 44000, Pakistan*
[6]*Department of Mathematical Economics, Faculty of International Relations and Economics, Baku State University, Baku, Azerbaijan*

Correspondence should be addressed to Jalil Manafian; j_manafianheris@tabrizu.ac.ir

Received 17 March 2022; Revised 19 May 2022; Accepted 26 May 2022; Published 25 June 2022

Academic Editor: Efstratios Tzirtzilakis

The flow of non-Newtonian fluids is extremely important in a variety of industrial applications and processes, including painting, printing, and coating. The goal of this paper is to develop a mathematical model for an incompressible, non-isothermal third-grade fluid as it travels through a minor gap between two heated rolls that are revolving in the opposite direction. Using appropriate dimensionless parameters, the dimensionless version of the governing equations is constructed. To simplify the nondimensional form of the governing equations, the LAT (lubrication approximation theory) is applied. It is mentioned that the perturbation approach should be used. It is a very important tool in modern mathematical physics and practical fluid mechanics, and it is used a lot. Through perturbation techniques, exact solutions for velocity distribution, flow rate, temperature distribution, and pressure gradient are offered. To observe the flow pattern, streamlines are also drawn. Numerical outcomes of some substantial engineering quantities like flow rate, roll separation force, power input, and pressure distribution are found. Some outcomes are displayed graphically although others are presented in tabular form. We have observed that the third-grade parameters give a way to control velocity, pressure gradients, flow rate, and coating thickness. Further, increasing the velocities ratio values lowers the coating thickness on the web. Furthermore, the Brickman number has a significant influence on the temperature profile and has increased with the increase in the Brickman number. Both the model and the numerical calculations are in agreement with the viscous fluid model that is already present in the literature.

1. Introduction

The analysis of non-Newtonian fluid flows has been enhanced due to its broad application in industry and engineering. Non-Newtonian fluids cannot simply be expressed as viscous fluids because all non-Newtonian fluids are not analyzed by a single constitutive equation. Several constitutive equations for this fluid have been developed because of this fact [1–11]. The modest subclass of non-Newtonian fluids is a second-grade fluid which can express the normal stress difference but cannot show the shear thinning/thickening characteristics. The fluid model named third-grade fluid attempts to include this characteristic of viscoelastic fluids. Third-grade fluids should be included in the family of grade fluids. The thermodynamics and stability theory of third-grade fluids have been established [12, 13]. They are viscoelastic, non-Newtonian fluids formed by an elastic and a viscous element, or, in other words, they are a mixture of a solvent and some polymers, such as DNA suspensions, paints, and some industrial and biological fluids. Polymers are found almost everywhere. While polymer suspensions exhibit viscoelastic properties, a single

model does not easily represent their stress-deformation relationship. We are using a constitutive model for third-grade fluid in this analysis as defined by Carapau et al. [14]. A higher-order differential equation is produced by the constitutive equation describing the relationship between the shear stress and the strain rate of a non-Newtonian fluid than in the classic Navier–Stokes equation. In addition, in many cases, the existing boundary conditions are smaller than the order of the differential equation. In order to deal with this complexity, researchers are looking for simple solutions. The well-known perturbation method is the most commonly used technique for approximate solutions. [15–18].

One of the analytical techniques for solving nonlinear differential equations is the perturbation technique. This approach is commonly used by engineers to solve some practical problems. At first, all perturbation techniques are focused on parameters that are small or big so that at least one unknown necessarily be represented in a series of minor (small) parameters. Third-grade material parameter beta β in this model and dynamic viscosity μ have the similar dimension, i.e., (kg/ms) (SI unit). In this research, we take very small β. The shear thickening or thinning relies on its numeric value. The material performs as a shear thickening substance if β is greater than zero. When β is smaller than zero, the substance material performs as a shear thinning material [18, 19].

Coating, or the depositing of a thin layer on a surface, has been used in a variety of applications for many years and is still being used today. If you think about it, make-up and painting are probably the oldest types of coating. Over time, they have become more sophisticated. Coatings are now used not only for decorative or protective purposes but also to improve the functionality of a surface or a substance by imparting functionality to them. For example, wrapping, photographic films, and food packaging films, whilst transparent, are coated with a gas barrier layer to limit the exposure of food to oxidation and moisture. The surface of paper is filled with a solution of mineral particles so that it can be printed clearly. Audio and video films are coated with a magnetic layer so that they can record and play back sound and images [20, 21]. In today's world, there are a lot of new applications being made, especially in the fields of healthcare, electronics, and energy capture. For example, optical films are used in liquid crystal displays (LCDs), plasma display panels (PDPs), and mobile phones; drug release patches are now being used to replace drugs that are injected or taken orally; and solar cells are coated with semiconducting layers to capture the energy of the sun and convert it into electricity. Coating as an industry is a truly massive, multi-billion-dollar worldwide enterprise that employs a large number of people all over the world and has gained a solid reputation in recent decades as a result of its widespread use in industry. It is unavoidably competitive, and as a result, it has gained a great deal of interest from researchers. These exercises make use of a diverse set of tools. Among these activities, roll coaters are frequently used [21–24].

In the technique of roll coating the distance between the two revolving rollers is substantially less than their radii. RRC (Reverse roll coating), FRC (forward roll coating), and metering roll coating are some of the most prevalent types of this technique [25]. Both with the reverse and metering rolls coating, the rolls at the minor gap (nip) go in opposite ways Wwhereas the both rolls at the minor gap move in the similar way for forward roll coating. After leaving the nip, the coating liquid creates a bath on the upstream side of the minor gap and separates into two liquid films, one of which is added to the web for industrial reasons and the other is protected by the both surfaces of the rollers [26, 27]. In [28], a few academics have focused on emergency situation research by the multicriteria group decision-making method, and the existing method has some areas for improvement.

The flow difficulties of roll coating processes have been investigated in depth over the last few decades, including theoretical work, experimental analysis, and numerical analysis. Among these, the FRC was of critical significance and was the subject of much discussion. Benkreira et al. [29] carried out an experimental research into this, [30, 31], while theoretical exploration has been offered by Benkreira et al. [26], Greener and Middleman et al. [30], Mücke et al. [32], and Alonso et al. [33]. In comparison to the forward roll coating investigation [34], RRC has acknowledged far less attention.

The LAT was used to simplify the motion equations in earlier studies of RRC systems by Greener and Middleman et al. [35] and Holland et al. [36], but the study of the association of the free surface, the effect of surface tension, and fluid contact lines were not taken into account. Coyle et al. [30] used a method of finite element supported by experimental outcomes to validate the essential properties of fluid dynamics for RRC. They also proved the presence of flow instabilities, including cascading and ribbing. The Galerkin finite element method is used by Hao et al. [27] to study the flow of coating between two reverse spinning rolls. Using the theory of lubrication approximation, Taylor and Zettlemoyer [37] investigated the behavior of ink flow during the printing press method. They were able to obtain the force and pressure distribution effects that they desired. Hinter Maier and White [38] addressed the flow of water among two rolls. They applied the LAT and gave results that matched their experimental data. A faultless RRC model was established by Belblidia et al. [21] using the Taylor–Galerkin pressure correction algorithm at maximum velocity. The innovation of the effort is inspired by the necessity from the coating manufacturing to uniform thin, faster, and coat stable layers, by coating rheology and operating coater operating conditions. The theoretical study of reverse roll coating of non-isothermal, an incompressible, magnetohydrodynamic viscoplastic fluid has been deliberated by Ali et al. [39]. The governing equation of flow added to the sheet in the basic form was achieved by employing the technique of lubrication approximation. The flow rate, velocity profile, and pressure gradient have all been shown to have analytical expressions. Williamson fluid was deliberated by Ali et al. [40] and thickness of coating, power input, pressure distribution, separation points, and roll separation force are some of the parameters of engineering interest that have been discussed. Zahid et al. [41] presented a mathematical model for the thin film roll coating process, which involves an incompressible Williamson material moving through a closed passage between a rotating roll and a web. They used an approach called regular

perturbation to provide an expression for the velocity profile, pressure gradient, flow rate per unit width, and shear stress at the roll surface. The findings of this study indicate that the operational variables are determined by the material factors that are involved. Authors of [42] analyzed the dynamics of ink at the liquid-air interface of coating bead and at the interface between the substrate and wet coated ink in a roll-to-roll slot die coating.

In the current study, a theoretical analysis of the third-grade fluid model was proposed during the reverse roll coating process. By utilizing LAT, the dimensionless form of the governing equation can be made more easily understood. The regular perturbation approach can be used to find closed-form solutions for velocity, temperature, and pressure gradient distributions. When determining coating thickness numerically, the Newton–Raphson method is typically employed. Also, the separation points, the force between the rolls when they separate, and the power that the rolls send to the fluid are all calculated numerically. Few of the outcomes are displayed in graphical form, while some are displayed in tabular form. The results show that the theoretical analysis is effective, novel, and correct. In recent years, different types of novel methods captured the attention of some researchers to solve nonlinear models such as complex-valued memristive neural networks [43], abrasive belt grinding considering residual stress [44], multi-dimensional prediction method [45], graphene/polyurethane composites coating [46], and ultrahigh molecular weight polyethylene fiber [47].

To our knowledge, there is no literature for a mathematical exploration of RRC for non-isothermal third-grade fluid. The current study's goal is to provide a theoretical investigation of the third-grade fluid as it passes between both heated rolls revolving in opposite directions.

2. Mathematical Formulation

Let us suppose the non-isothermal, an incompressible, steady flow of a third-grade fluid. The two rolls with the identical radii R are parallel to each other and situated in the plane of the free surface that rotates reversely with peripheral velocities of U_r and U_f, where the subscripts r and f are stand for reverse and forward rotating rolls, respectively. A thin gap between the revolving rolls is maintained known as the nip region, which is symbolized by $2H_0$. In the minor area termed as nip among the two rolls, the coating flow is drawn via the reverse roll. Additionally, the $x-$ axis and $y-$ axis are taken alongside and transverse to the flow movement, as presented in Figure 1.

The following are the fundamental equations that regulate the flow of a non-isothermal, steady fluid [48–50]:

$$\begin{aligned} &\operatorname{div}\mathbf{U} = 0,\\ &\rho\frac{\mathrm{D}\mathbf{U}}{\mathrm{D}t} = -\nabla p + \operatorname{div}\mathbf{T},\\ &\rho C_p\frac{\mathrm{D}\theta}{\mathrm{D}t} = k\nabla^2\theta + \boldsymbol{\tau}\cdot\mathbf{L}, \end{aligned} \tag{1}$$

where ρ is the density of the fluid, C_p stands for the specific heat capacity, θ is the temperature, $\mathbf{L} = \nabla\mathbf{U}$ is the velocity gradient, k denotes the thermal conductivity, $\mathbf{U}$ is the fluid velocity, $(D/\mathrm{D}t)$ denotes the material time derivative, and the extra stress tensor is denoted by $\mathbf{T}$ for third-grade fluid [51] which satisfies the constitutive equation as follows:

$$\begin{aligned} \mathbf{T} &= \mu\mathbf{A}_1 + \alpha_1\mathbf{A}_2 + \alpha_2\mathbf{A}_1^2 + \beta_1\mathbf{A}_3\\ &\quad + \beta_2\left(\mathbf{A}_1\mathbf{A}_2 + \mathbf{A}_2\mathbf{A}_1\right) + \beta_3\left(tr\mathbf{A}_1^2\right)\mathbf{A}_1,\\ \frac{\mathrm{D}(\cdot)}{\mathrm{D}t} &= \frac{\partial(\cdot)}{\partial t} + (\mathbf{U}\cdot\nabla)(\cdot),\\ \mathbf{A}_1 &= (\nabla\mathbf{U}) + (\nabla\mathbf{U})^T,\\ \mathbf{A}_n &= \left(\frac{\partial}{\partial t} + (\nabla\cdot\mathbf{U})\right)\mathbf{A}_{n-1} + \mathbf{A}_{n-1}(\nabla\mathbf{U}) + (\nabla\mathbf{U})^t\mathbf{A}_{n-1}. \end{aligned} \tag{2}$$

where μ denotes the dynamic viscosity, $A_i\,(i = 1, 3)$ are denotes the first three Rivlin-Ericksen tensors, $\alpha_i\,(i = 1, 2)$ and $\beta_i\,(i = 1, 3)$ stand for the material constants and t specifies the matrix transpose. Equation (4) is converted to second-grade fluid when β_1, β_2, and β_3 are zero and converted to the Newtonian fluid model when all material moduli except μ are zero. The velocity profile for fluid flow is as follows:

$$\mathbf{U} = [u(x, y), v(x, y), 0]. \tag{3}$$

We start with the LAT that the most significant dynamic events happen in the nip region of reverse roll coating procedure. In that area, enlarging to any side by a small distance, the surface of the roll is almost parallel. Then, it is equitable to take up that $u > v$ and $(\partial/\partial y) > (\partial/\partial x)$. The material travels in the $x-$ direction, and there is no velocity that can be observed in the $y-$ direction. This conversation leads equation (2) into the following component form:

$$\frac{\mathrm{d}S_{xy}}{\mathrm{d}y} - \frac{\partial p}{\partial x} = 0, \tag{4}$$

$$\frac{\mathrm{d}S_{yy}}{\mathrm{d}y} - \frac{\partial p}{\partial y} = 0, \tag{5}$$

where

$$\begin{aligned} S_{xy} &= \frac{\mathrm{d}u}{\mathrm{d}y} + 2(\beta_2 + \beta_3)\left(\frac{\mathrm{d}u}{\mathrm{d}y}\right)^3,\\ S_{yy} &= (2\alpha_1 + \alpha_2)\left(\frac{\mathrm{d}u}{\mathrm{d}y}\right)^2. \end{aligned} \tag{6}$$

On defining generalized pressure P,

$$P(x, y) = p(x, y) - (2\alpha_1 + \alpha_2)\left(\frac{\mathrm{d}u}{\mathrm{d}y}\right)^2. \tag{7}$$

Inserting (6) and (7), (4) and (5) take the form as

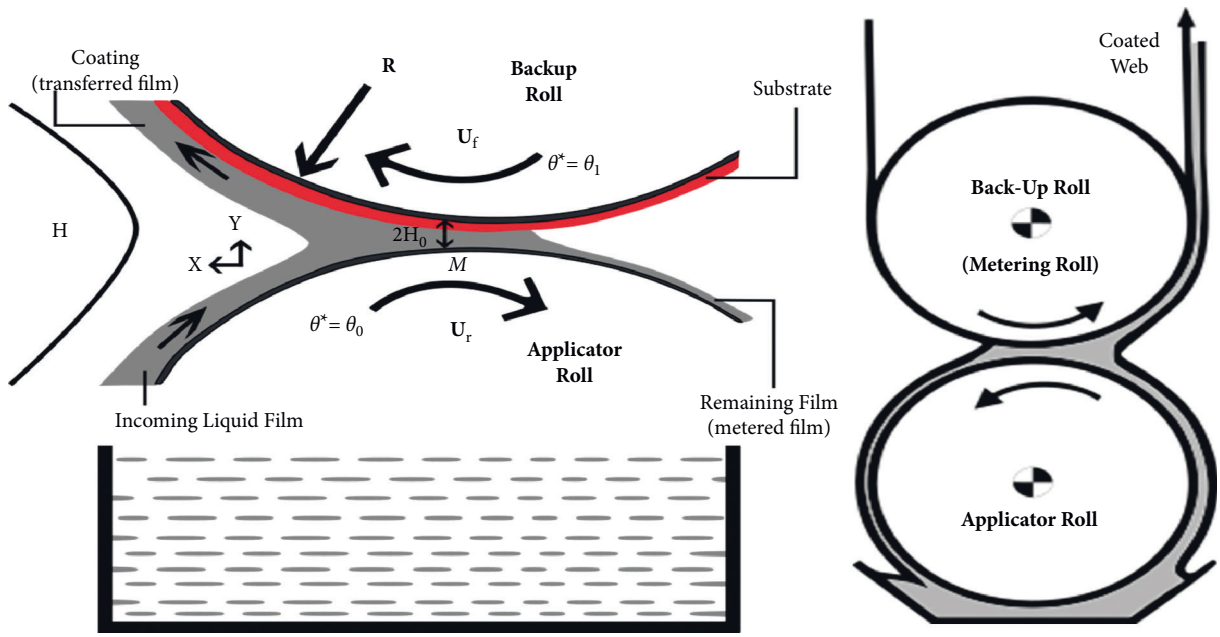

Figure 1: Geometry of reverse roll coating.

$$\mu\frac{d^2u}{dy^2} + 2(\beta_2+\beta_3)\frac{d}{dy}\left(\frac{du}{dy}\right)^3 = \frac{\partial P}{\partial x},$$

$$\frac{\partial P}{\partial y} = 0, \tag{8}$$

$$k\frac{d^2\theta}{dy^2} + \mu\left(\frac{du}{dy}\right)^2 + 2(\beta_2+\beta_3)\left(\frac{du}{dy}\right)^4 = 0.$$

Form equation (14), it is obvious that P is a function of x. So, equation (13) can be rewritten as

$$\mu\frac{d^2u}{dy^2} + 2\beta_4\frac{d}{dy}\left(\frac{du}{dy}\right)^3 = \frac{dP}{dx}, \tag{9}$$

$$k\frac{d^2\theta}{dy^2} + \mu\left(\frac{du}{dy}\right)^2 + 2\beta_4\left(\frac{du}{dy}\right)^4 = 0. \tag{10}$$

For simplicity, we have introduced $\beta_4 = \beta_2 + \beta_3$.

2.1. Dimensionless Equation. The governing equations of third-grade fluid during RRC procedure are presented in nondimensional form in this section. Assume the following dimensionless variables are appropriate [27, 38]:

$$x^* = \frac{x}{\sqrt{RH_0}}, u^* = \frac{u}{U_f}, y^* = \frac{y}{H_0},$$

$$P^* = \sqrt{\frac{H_0}{R}}\,\frac{PH_0}{\mu U_f}, \beta = \frac{2\beta_4 U_f^2}{\mu H_0}, \tag{11}$$

$$h^*(x^*) = \frac{h(x)}{H_0}, \theta^* = \frac{\theta-\theta_0}{\theta_1-\theta_0}.$$

In view of above dimensionless variables, (9) and (10) can be written as after removing $'*'$

$$\frac{d^2u}{dy^2} + \beta\frac{d}{dy}\left(\frac{du}{dy}\right)^3 = \frac{dP}{dx}, \tag{12}$$

$$\frac{d^2\theta}{dy^2} + \Upsilon\left(\frac{du}{dy}\right)^2 + \beta\Upsilon\left(\frac{du}{dy}\right)^4 = 0, \tag{13}$$

where $\Upsilon = (\mu C_p/k) \times (U_f^2/C_p(\theta_1-\theta_0)) = \mathrm{EcPr}$; here, Ec and Pr represent the Eckert and Prandtl number, respectively, and their product represents the Brickman number Υ. The Brickman number signifies a quantity of the significance of the viscous heating comparaing the conductive heat transfer.

Dimensionless kinematic boundary condition that is appropriate [35] is

$$\left.\begin{aligned} u &= 1 \text{ at } y = -\sigma \\ u &= -K \text{ at } y = \sigma \\ \theta &= 0 \text{ at } y = -\sigma \\ \theta &= 1 \text{ at } y = \sigma \end{aligned}\right\}, \tag{14}$$

where $K = (U_r/U_f)$ and the boundary of roll surface is represented as $y = \pm\sigma(x) = 1 + (x^2/2)$.

3. Solution for $\beta \ll 1$

As a result of the fact that the majority of mathematical problems do not have explicit answers, it is of the utmost significance to be familiar with techniques that can approximate the answers to such sorts of problems. An effective method for obtaining approximate solutions to difficult problems is provided by asymptotic analysis, which can be used in combination with the perturbation technique.

When dealing with problems that contain a parameter that is either extremely large or extremely small, it is important to make use of the structure of the problem in order to achieve the most accurate approximation possible. These methods are extremely helpful when dealing with converging and diverging geometries, such as coating flow problems. Due to the fact that (12) is a nonlinear differential equation, finding a solution in closed form can be challenging. Therefore, the solution of nonlinear differential equation given in (12) is obtained analytically by using regular perturbation technique for $\beta \ll 1$ (as a parameter for perturbation) and expanding the velocity u, pressure p, pressure gradient $(\mathrm{d}p/\mathrm{d}x)$, temperature distribution θ, and dimensionless film thickness in the power series of β:

$$\begin{aligned} u &= u_0 + \beta u_1 + \beta^2 u_2 + O\left(\beta^3\right), \\ \frac{\mathrm{d}p}{\mathrm{d}x} &= \frac{\mathrm{d}p_0}{\mathrm{d}x} + \beta\frac{\mathrm{d}p_1}{\mathrm{d}x} + \beta^2\frac{\mathrm{d}p_2}{\mathrm{d}x} + O\left(\beta^3\right), \\ P(x) &= P_0(x) + \beta P_1(x) + \beta^2 P_2(x) + O\left(\beta^3\right), \\ \lambda &= \lambda_0 + \beta\lambda_1 + \beta^2\lambda_2 + O\left(\beta^3\right), \\ \theta &= \theta_0 + \beta\theta_1 + \beta^2\theta_2 + O\left(\beta^3\right), \end{aligned} \tag{15}$$

where u_0, $(\mathrm{d}p_0/\mathrm{d}x)$, P_0, θ_0, and λ_0 are the leading-order solutions, which characterize the Newtonian model and u_1, P_1, u_0, $(\mathrm{d}p_1/\mathrm{d}x)$ θ_1, λ_1, u_2, P_2, $(\mathrm{d}p_2/\mathrm{d}x)$, θ_2, and λ_2 are the corrections up to second-order terms and comprise the influence of the non-Newtonian consequence. By plugging the expressions (22) to (26) into equations (19) and (20) and equating like powers of β, we are able to derive the following set of problems.

For β^0,

$$\frac{\mathrm{d}^2 u_0}{\mathrm{d}y^2} = \frac{\mathrm{d}P_0}{\mathrm{d}x}, \tag{16}$$

with boundary conditions

$$\begin{aligned} u_0 &= 1 \text{ at } y = -\sigma, \\ u_0 &= -K \text{ at } y = \sigma. \end{aligned} \tag{17}$$

For β^1,

$$\frac{d^2 u_1}{\mathrm{d}y^2} + \frac{d}{\mathrm{d}y}\left(\frac{\mathrm{d}u_0}{\mathrm{d}y}\right)^3 = \frac{\mathrm{d}p_1}{\mathrm{d}x}, \tag{18}$$

with boundary condition

$$\begin{aligned} u_1 &= 0 \text{ at } y = \sigma, \\ u_1 &= 0 \text{ at } y = -\sigma. \end{aligned} \tag{19}$$

3.1. Zeroth-Order Solution. The solution of (16) with (17) is given by

$$u_0 = \frac{1}{2}\left(y^2 - \sigma^2\right)\frac{\mathrm{d}p_0}{\mathrm{d}x} - \frac{1}{2\sigma}(1+K)y - \frac{1}{2}(K-1). \tag{20}$$

The zero-order flow rate in dimensionless is defined as

$$\lambda_0 = \frac{1}{2}\int_{-\sigma}^{\sigma} u_0(y)\mathrm{d}y. \tag{21}$$

From (20) and (21), we get

$$\frac{\mathrm{d}p_0}{\mathrm{d}x} = -\frac{3\left((K-1)\sigma + 2\lambda_0\right)}{2\sigma^3}. \tag{22}$$

And,

$$p_0(x) = \frac{1}{16\left(x^2+2\right)^2}\begin{pmatrix} -18\sqrt{2}\left(\lambda_0 + \frac{2}{3}(K-1)\right)\left(x^2+2\right)^2 \arctan\left(\frac{x\sqrt{2}}{2}\right) \\ -9\pi\sqrt{2}\left(\lambda_0 + \frac{2}{3}(K-1)\right)\left(x^2+2\right)^2 - 36\left(\left(\lambda_0 + \frac{2}{3}(K-1)\right)x^2 + \frac{10}{3}\lambda_0 + \frac{4}{3}(K-1)\right)x \end{pmatrix}. \tag{23}$$

In order to find values for $\lambda_0(K)$, the Swift–Stieber boundary condition on pressure will be imposed. It is asserted that at the transition point $x = x_t$ where a lubrication type flow offers way to a transvers flow, both the pressure and the pressure gradient vanished. On setting $(\mathrm{d}p_0/\mathrm{d}x) = 0$ in (22), we get

$$\sigma_t = 1 + \frac{x_t^2}{2} = \frac{2\lambda_0}{1-K}, \tag{24}$$

when the left hand side of (23) is set equal to zero and (24) is used to replace x by x_t. We get a transcendental equation in zero-order flow rate λ_0, which is solved by using a numerical method called Newton–Raphson method. The results are shown in Tables 1 and 2

3.2. First-Order Solution. The solution process is alike to zero-order solution. Upon using (20) into (18) and solved with help of (19), we get

Table 1: Variation in dimensionless flow rate with respect to separation points.

x_t	λ
0	−0.097865369
0.1	−0.094456027
0.2	−0.084732531
0.3	−0.070041696
0.4	−0.052159590
0.5	−0.032832053
0.6	−0.013450446
0.7	0.0050658080
0.8	0.022218913
0.9	0.0337803413
1	0.051775686

Table 2: Effect of K on flow rate, separation points, coating thickness, power input, and force.

K	λ	x_t	v	p_w	F
0.1	0.5446	0.5937	1.0803	−1.6789	0.5601
0.2	0.4825	0.5935	1.0685	−1.8482	0.4985
0.3	0.4207	0.5934	1.0573	−2.0228	0.4371
0.4	0.3593	0.5933	1.0467	−2.2039	0.3754
0.5	0.2984	0.5932	1.03712	−2.3923	0.3133
0.6	0.2378	0.5931	1.0280	−2.5880	0.2511
0.7	0.1776	0.5930	1.0197	−2.7908	0.1888
0.8	0.1178	0.5925	1.0120	−3.0011	0.1263
0.9	0.0587	0.5910	1.0057	−3.2207	0.0635

$$u_1(y) = -\frac{1}{8\sigma^2}\left(3\left(\begin{array}{c} -\dfrac{9(K\sigma+2Q-\sigma)}{4\sigma^5}+\left(-\dfrac{9(K\sigma+2Q-\sigma)y^2}{4\sigma^9}-\dfrac{4}{3}\dfrac{dp_1}{dx}\right)\sigma^2- \\ \\ \dfrac{3(K\sigma+2Q-\sigma)}{\sigma^5}\left((K+1)y-(K+1)^2\right) \end{array}\right)(y+\sigma)(y-\sigma)\right). \tag{25}$$

The first-order flow rate in dimensionless form is defined as

$$\lambda_1 = \frac{1}{2}\int_{-\sigma}^{\sigma} u_1(y)\,dy. \tag{26}$$

From (25) and (26), we have

$$\frac{dp_1}{dx} = \frac{-60\lambda_1\sigma^4+\left(-63K^3+99K(K-1)+63\right)\sigma^3-288\lambda_0\left(K^2-11/8K+1\right)\sigma^2-486\lambda_0^2(K-1)\sigma}{20\sigma^7}. \tag{27}$$

And first-order pressure distribution is found by integrating (27) with boundary condition $p_1 = 0$ as $x \longrightarrow -\infty$.

A second simple material balance relationship for λ is defined as

$$U_f H_f - U_r H_r = 2\lambda H_0 U_f, \tag{28}$$

where U_f and U_r are velocities for forward and reverse roll, respectively.

Equation (28) led to the expression which is given by

$$v = \frac{H_f}{H_r} = K + 2\Upsilon\lambda, \tag{29}$$

where $v = (H_f/H_r)$ is the coating thickness, $\Upsilon = (H_0/H_r)$, where H_0 is half the nip separation area among two rolls, and H_f and H_r denote the fluid film thickness on the forward and reverse roll, respectively. So, we necessity to find the value of flow rate $\lambda(K)$ to compute the pressure distribution and thickness of coating.

To determine the value of $\lambda_1(K)$, enforce Swift-Stieber boundary conditions on pressure distributions. It is asserted

that at the separation point $x = x_t$ where the lubrication type flow transforms into a transverse flow, both the pressure and pressure gradient vanished. On setting $(dp_1/dx) = 0$ in (27), we need an explicit relation among the separation point and dimensionless flow rate $\lambda_1(K)$. It is impossible to find this relationship for the constitutive model under consideration. The data points can easily be produced to interpolate the required polynomial from the implicit relationship among the dimensionless coating thickness λ_1 and separation points.

Table 1 is the created data for $K = 0.1$. In terms of coating thickness λ_1, a 10-degree interpolating polynomial has been established, which has been further used in the resulting equation from (27) for pressure distributions in order to calculate the thickness of coating. After utilizing the created explicit relation among separation points in terms of flow rate into resulting equation from (27) for pressure distributions, a transcendental equation in flow arte λ_1 has been obtained. The numerical method known as the Newton–Raphson method is used to obtain results for λ_1.

Table 3: Effect of β on flow rate, separation points, coating thickness, power input, and force.

β	λ	x_t	v	p_w	F
0.1	0.4887	0.6620	1.0796	−1.7483	0.4905
0.2	0.4872	0.6522	1.0769	−1.7834	0.4918
0.3	0.4856	0.6424	1.0741	−1.8146	0.4932
0.4	0.4841	0.6326	1.0714	−1.8418	0.4949
0.5	0.4825	0.6229	1.0685	−1.8656	0.4969
0.6	0.4810	0.6131	1.0658	−1.8857	0.4990
0.7	0.4794	0.6034	1.06291	−1.9025	0.5014
0.8	0.4779	0.5935	1.0602	−1.9159	0.5039
0.9	0.4763	0.5837	1.0573	−1.9263	0.5067

4. Temperature Distribution

Upon using equation (22) into the dimensionless form of energy (13), we get

$$\frac{d^2\theta_0}{dy^2} + \beta\frac{d^2\theta_1}{dy^2} + \Upsilon\left(\frac{du_0}{dy} + \beta\frac{du_1}{dy}\right)^2 + \beta\Upsilon\left(\frac{du_0}{dy} + \beta\frac{du_1}{dy}\right)^4 = 0,$$
$$\frac{d^2\theta_0}{dy^2} + \beta\frac{d^2\theta_1}{dy^2} + \Upsilon\left(\left(\frac{du_0}{dy}\right)^2 + \beta^2\left(\frac{du_1}{dy}\right)^2 + 2\beta\frac{du_0}{dy}\frac{du_1}{dy} + \beta\left(\frac{du_0}{dy}\right)^4 + 0\left(\beta^2\right)\right) = 0. \tag{30}$$

On ignoring higher order of β, we get

$$\frac{d^2\theta_0}{dy^2} + \beta\frac{d^2\theta_1}{dy^2} + \Upsilon\left(\left(\frac{du_0}{dy}\right)^2 + 2\beta\frac{du_0}{dy}\frac{du_1}{dy} + \beta\left(\frac{du_0}{dy}\right)^4\right) = 0. \tag{31}$$

Comparing coefficient of β^0 and β^1, we get

$$\frac{d^2\theta_0}{dy^2} + \Upsilon\left(\frac{du_0}{dy}\right)^2 = 0,$$
$$\frac{d^2\theta_1}{dy^2} + 2\Upsilon\frac{du_0}{dy}\frac{du_1}{dy} + \Upsilon\left(\frac{du_0}{dy}\right)^4 = 0. \tag{32}$$

4.1. Zero-Order Problem and Its Solution. The zero-order BVP (boundary value problem) is

$$\frac{d^2\theta_0}{dy^2} + \Upsilon\left(\frac{du_0}{dy}\right)^2 = 0. \tag{33}$$

$$\left.\begin{aligned}\theta_0 &= 0 \text{ at } y = -\sigma\\ \theta_0 &= 1 \text{ at } y = \sigma\end{aligned}\right). \tag{35}$$

The solution of (34) with the help of (35) is

$$\theta_0 = -\frac{(y+\sigma)\left(\left(2/3\left(dp_0/dx\right)^2\sigma^2\left(\sigma^2+y^2\right) - 4/3\left(dp_0/dx\right)y(K+1)\sigma + (K+1)^2\right)(y-\sigma)\Upsilon - 4\sigma\right)}{8\sigma^2}. \tag{35}$$

4.2. First-Order Problem and Its Solution. The first-order BVP is given by

$$\left.\begin{aligned} \frac{d^2\theta_1}{\mathrm{d}y^2} + 2\Upsilon\frac{\mathrm{d}u_0}{\mathrm{d}y}\frac{\mathrm{d}u_1}{\mathrm{d}y} + \Upsilon\left(\frac{\mathrm{d}u_0}{\mathrm{d}y}\right)^4 = 0, \\ \theta_1 = 0 \text{ at } y = -\sigma \\ \theta_1 = 0 \text{ at } y = \sigma \end{aligned}\right). \tag{36}$$

The solution of above problem is

$$\theta_1 = -\frac{1}{32\sigma^4}\left[\left[\begin{array}{l} \frac{16p\sigma^5}{15}\left(-p^3\sigma^3 - \left(p^3y^2 - 5q\right)\sigma - 2p^2y(K+1)\right) \\ +4\left(-\frac{4p^3y^4}{15} + \frac{4qy^2}{3} + p(K+1)^2\right)p\sigma^4 \\ +\frac{16\left(p^3y^2 - (5q/3)\right)(K+1)y\sigma^3}{5} - 4p^2y^2(K+1)^2\sigma^2 \\ +\frac{4py(K+1)^3}{3}\sigma + (K+1)^4 \end{array}\right](y+\sigma)(y-\sigma)\Upsilon\right]. \tag{37}$$

As a result, up to first order, the perturbation solution is as follows:

$$\left.\begin{aligned} u &= u_0 + \beta u_1 \\ \lambda &= \lambda_0 + \beta\lambda_1 \\ \frac{\mathrm{d}p}{\mathrm{d}x} &= \frac{\mathrm{d}p_0}{\mathrm{d}x} + \beta\frac{\mathrm{d}p_1}{\mathrm{d}x} \\ \theta &= \theta_0 + \beta\theta_1 \end{aligned}\right), \tag{38}$$

where $u_0, u_1, (\mathrm{d}p_0/\mathrm{d}x), (\mathrm{d}p_1/\mathrm{d}x), \theta_0$, and θ_1 are given in (20), (36), (33), (38), (36), and (38), respectively.

5. Operating Variables

Operating factors like power input and separation force can be straightforwardly found when the pressure distributions, velocity profile, and pressure gradients have been obtained.

5.1. Separating Force. The dimensionless force of roll separating F is given by

$$F = \frac{\overline{F}H_0}{\mu\,\mathrm{URW}} = \int_{-\infty}^{x_t} p(x)\mathrm{d}x, \tag{39}$$

where $\overline{F}$ and F denote the dimensional and dimensionless force of roll separating per unit width W, respectively.

5.2. Power Input. The power transferred by the rolls to the fluid is obtained by integral

$$p_w = \frac{\overline{P}}{\mu\,\mathrm{WU}^2} = \int_{-\infty}^{x_t} \tau_{\mathrm{xy}}(x,1)\mathrm{d}x. \tag{40}$$

Here, P_w symbolizes the nondimension power.

6. Result and Discussion

The theoretical investigations of third-grade (viscoelastic) fluid for the phenomena of reverse roll coating have been studied in this article. LAT is employed to make simpler the nondimension form of the governing equations. The numeric results for separation points x_t, flow rate λ, power input p_w, coating thickness υ, and roll separation force F for numerous values of velocities ratio K and third-grade parameter β are shown in Tables 2–4. It is observed from Tables 2 and 3 that the thickness of coating, flow rate, and separation points are the decreasing functions for the rising values of K and β, respectively. Also, the magnitude of power input rises although the roll separation force is decreasing with an rise in K. It has been observed from Table 4 that the thickness of coating is increased by rising the nip gap. We found that when $\beta \longrightarrow 0$, all the results of [27] are retrieved.

Table 4: Effect of $\Upsilon = (H_0/H_r)$ on coating thickness.

$K = 0.1$, $\lambda = 0.5446$, $\Upsilon = (H_0/H_r)$	υ	$K = 0.3$, $\lambda = 0.4207$, $\Upsilon = (H_0/H_r)$	υ	$K = 0.5$, $\lambda = 0.2984$, $\Upsilon = (H_0/H_r)$	υ
0.1	0.2089	0.1	0.3841	0.1	0.5597
0.2	0.3178	0.2	0.4683	0.2	0.6194
0.3	0.4267	0.3	0.5524	0.3	0.6790
0.4	0.5357	0.4	0.6365	0.4	0.7387
0.5	0.6446	0.5	0.7207	0.5	0.7984
0.6	0.7535	0.6	0.8048	0.6	0.8581
0.7	0.8624	0.7	0.8889	0.7	0.9177
0.8	0.9714	0.8	0.9731	0.8	0.9774
0.9	1.0803	0.9	1.05793	0.9	1.0371

The dimensionless velocity profile outcomes for various values of K and β at different position of x $(0, 0.5, 0.75)$ are presented in Figures 2–7. The velocity in Figure 2 has been outlined at the nip area $(x = 0)$ for the various values of K in the domain $[0.1, 0.9]$. It has been found that the velocity profile declines when the velocities ratio K values are increased. On the revere roll surface, the maximum velocity was observed. When travelling in the forward roll direction, it starts to decline and eventually reaches zero while $y \in [0.005, 0.865]$; after this domain, depending on the value of K and in the direction of the coating web, there is a reverse flow. From Figures 3 and 4 can be understood that when travelling in the way of the separation point, at various points during the RRC procedure, the domain of y, where the fluid velocity extents to zero rises, after that this domain depending on the values of velocities ratio K, while traveling in the direction of the upper roll, the velocity magnitude rises and achieve its highest velocity at the roll surface. Here, it is highlighted that for small K, consistency with the model's predictions is ideal whereas for larger K compared with unity, deviances increase. Figures 5–7 show the velocity results for the several values of β at several positions in the reverse roll coating process. It has been perceived from these figures that the velocity of the fluid decreases by rising the value of β. When seen from a physical perspective, this indicates that an increase in the third-grade parameter β corresponds to the result of the fluid becoming more viscous and that an increase in the third-grade parameter results in a corresponding increase in the viscosity of the liquid. As a direct result of this, the magnitude of the fluid velocity will be reduced.

The graphical results for pressure gradient (dp/dx) versus the axial coordinate x for the involved parameters such as K (velocities ratio) and β (non-Newtonian parameter) from 0.1 to 0.9 are presented in Figures 8-9. It is clear from these figures that the absolute value of the pressure gradients declines for increasing values of K although opposite manners have been noted for the rising value of β.

The nondimension graphical illustrations of pressure distributions for the several values of K and β are drawn in Figures 10 and 11, respectively. From Figure 10, it is witnessed that when one can begin moving in the direction of the negative $x - axis$, the value of pressure distribution increases and becomes zero at attachment points. Also, one can observe from Figure 11 that the pressure distribution increases as β increases.

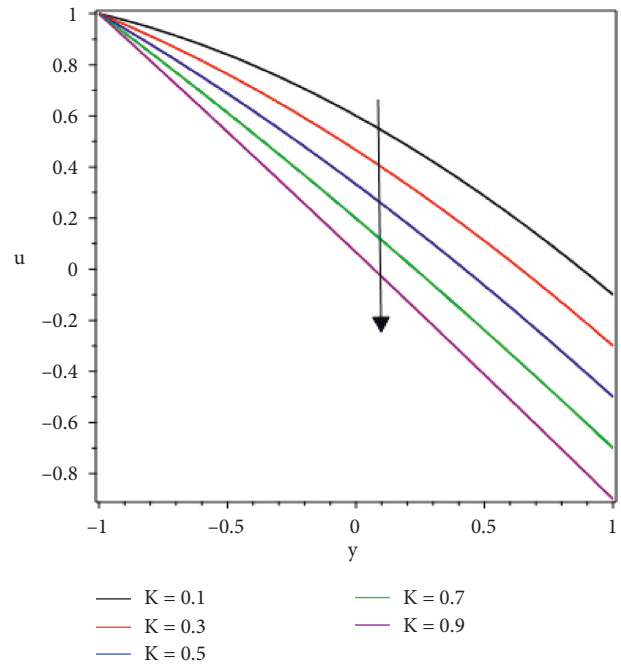

Figure 2: Impact of K upon velocity distribution at $x = 0$.

The influence of involved parameters like K, β, and Brickman number Υ on dimensionless temperature profile is outlined in Figures 12–17 at different situations in reverse roll coating procedure. Figures 12 and 13 are drawn at $x = 0$ and $x = 0.75$ for rising values of K whereas β and Υ are kept fixed. It has been perceived that for rising value of K, the temperature profile increases. Similar behavior is observed from Figures 14–17 for the rising values of third-grade parameter β and Υ, i.e. increase in these parameters results in the rise of temperature. Physically it means that the Brickman number Υ is a nondimensional quantity that is associated with the transfer of heat from the roll to the coating fluid. Brickman's number is the ratio of the heat that is generated by viscous dissipation to the heat that is transferred by molecular conduction; alternatively, it is the ratio of the heat that is generated by viscous dissipation to the heat that is generated by external warming. The greater the value is, the more slowly heat will be transmitted by viscous dissipation, and the greater the temperature increase will be as a result.

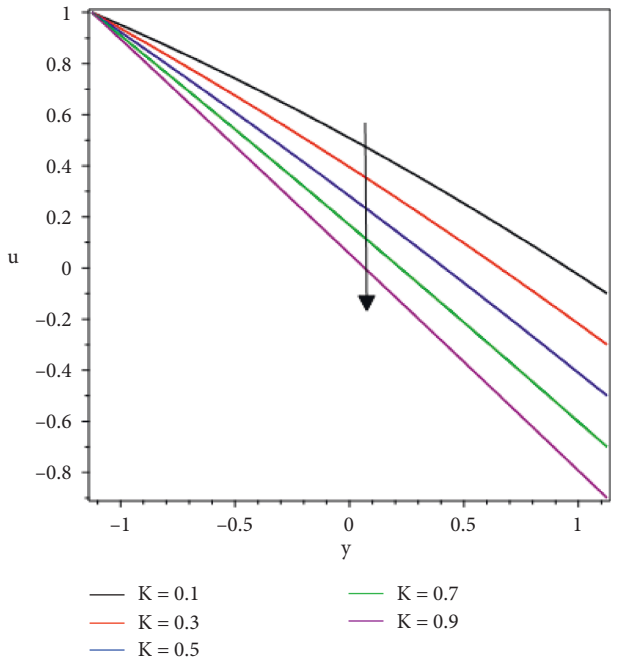

Figure 3: Impact of K upon velocity distribution at $x = 0.5$.

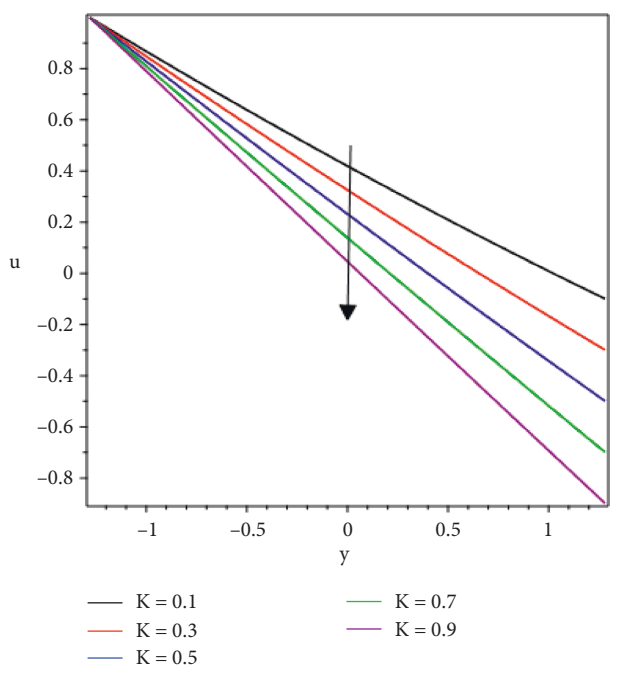

Figure 4: Impact of K upon velocity distribution at $x = 0.75$.

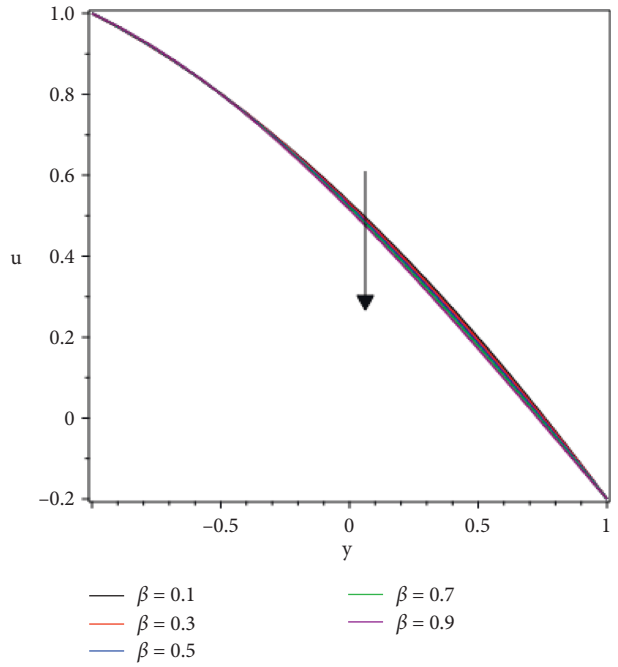

Figure 5: Impact of β upon velocity distribution at $x = 0$.

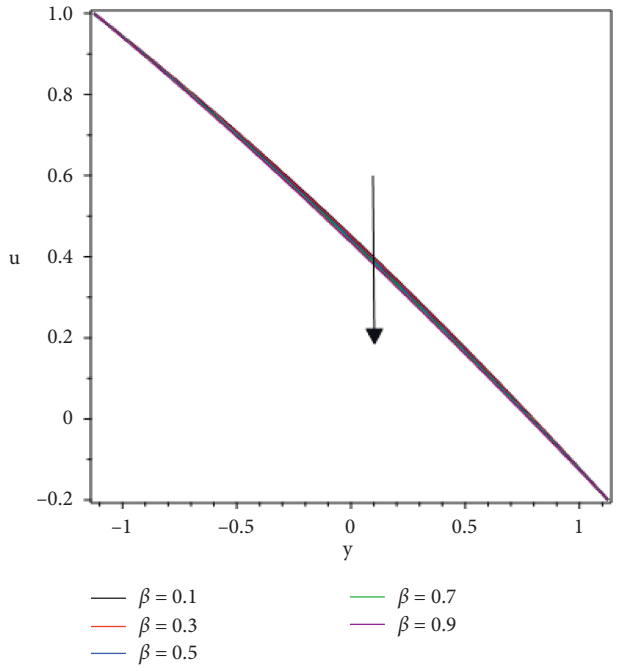

Figure 6: Impact of β upon velocity distribution at $x = 0.5$.

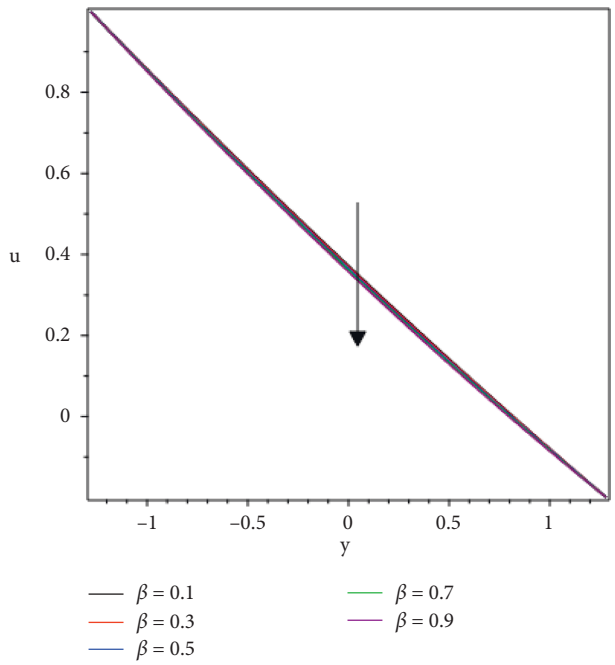

Figure 7: Impact of β upon velocity distribution at $x = 0.75$.

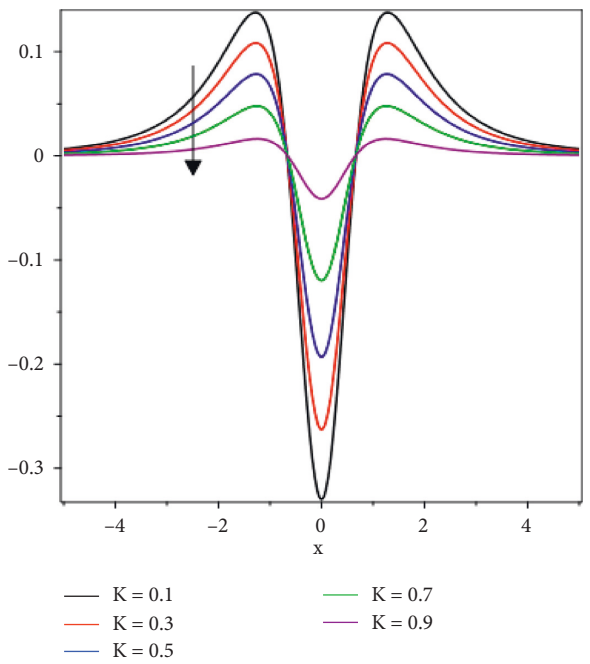

Figure 8: Impact of K upon pressure gradient distributions.

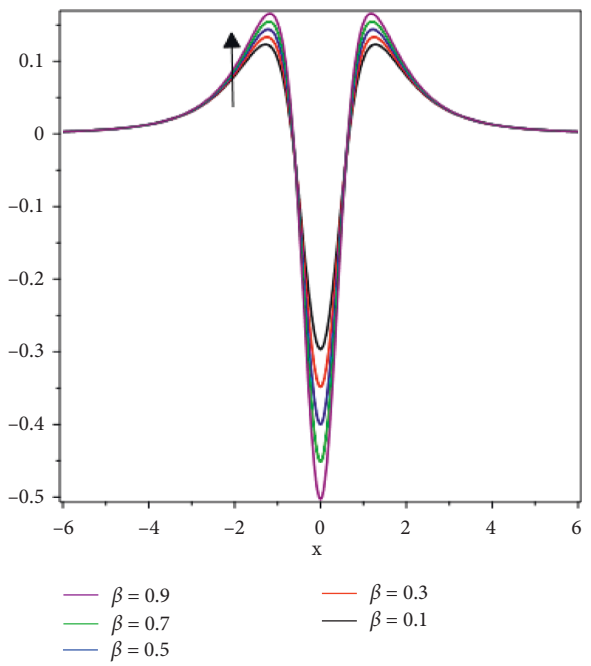

Figure 9: Impact of β upon pressure gradient distributions.

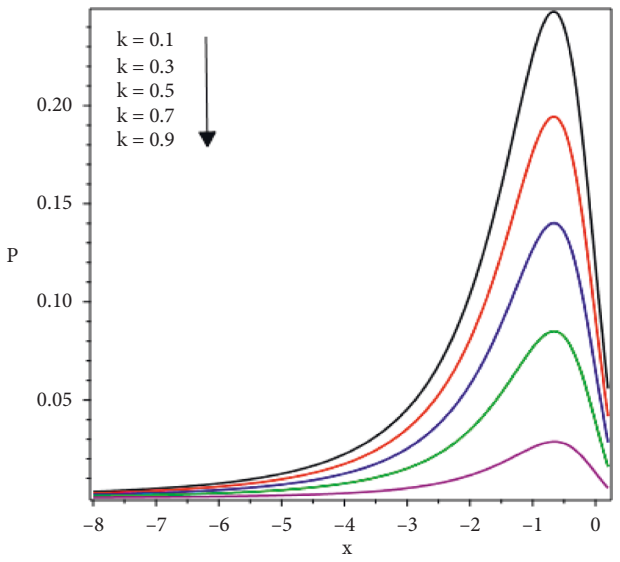

Figure 10: Impact of K upon pressure distributions.

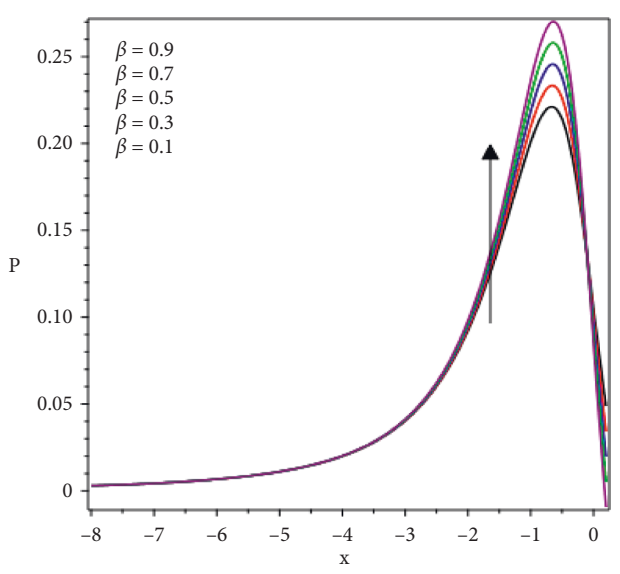

Figure 11: Impact of β upon pressure distributions.

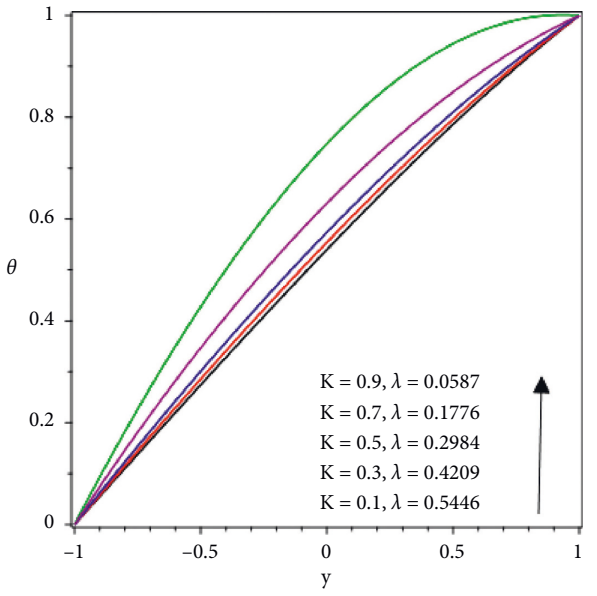

Figure 12: Impact of K upon temperature distribution at $x = 0$.

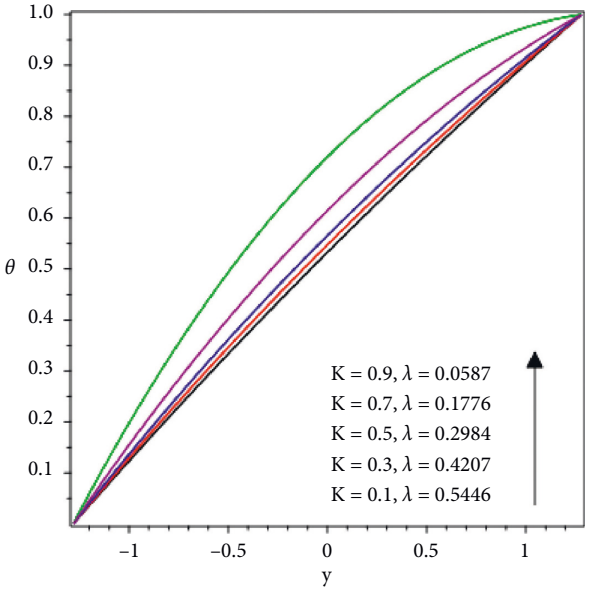

Figure 13: Impact of K upon temperature at $x = 0.75$.

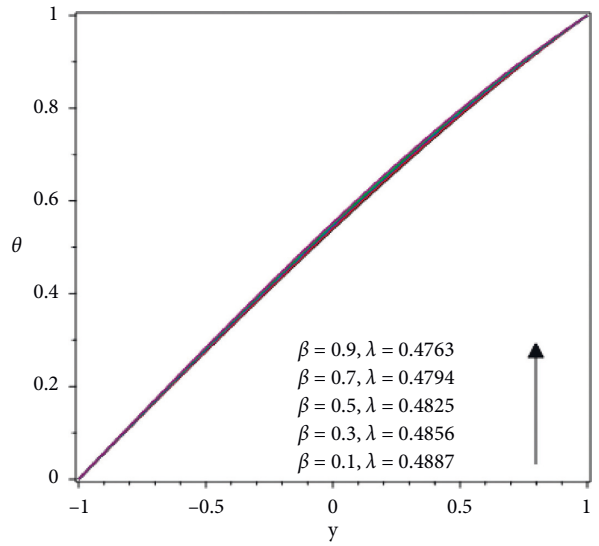

Figure 14: Impact of β upon temperature distribution at $x = 0$.

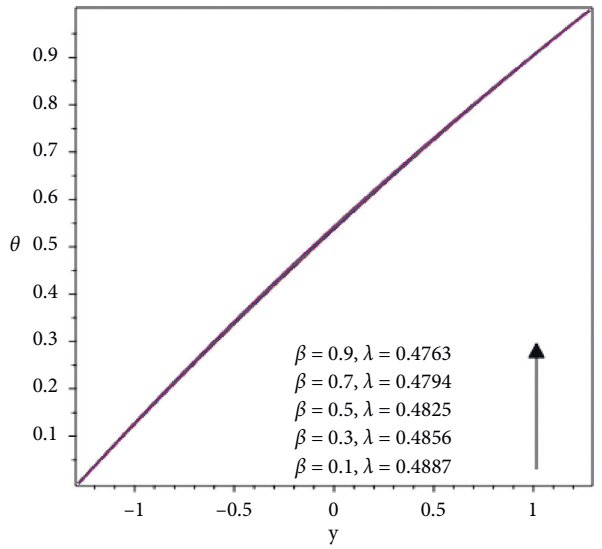

Figure 15: impact of β upon temperature distribution at $x = 0.75$.

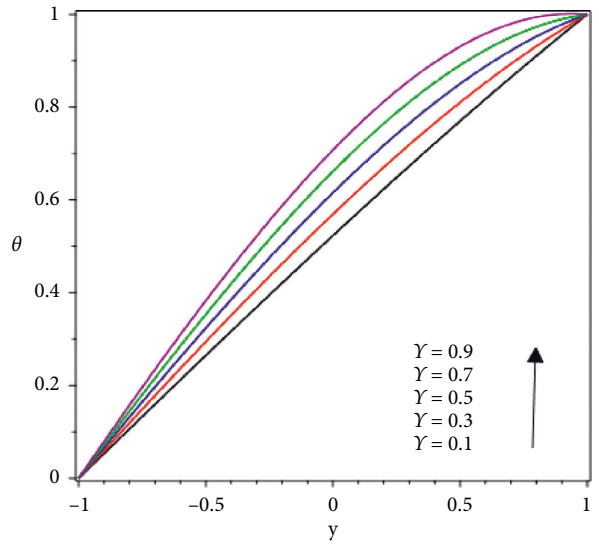

Figure 16: Impact of Υ upon temperature distribution at $x = 0$.

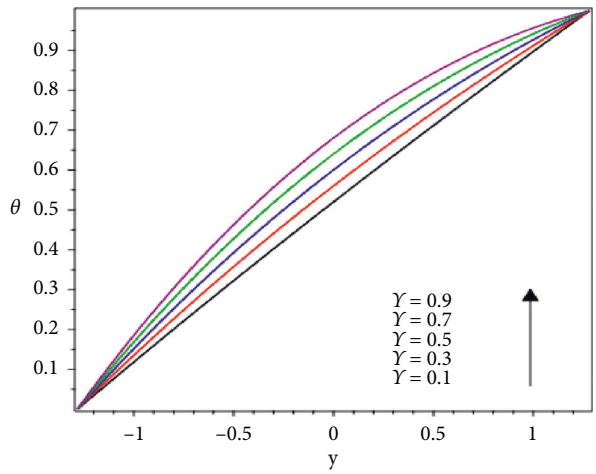

Figure 17: Impact of Υ upon temperature distribution at $x = 0.75$.

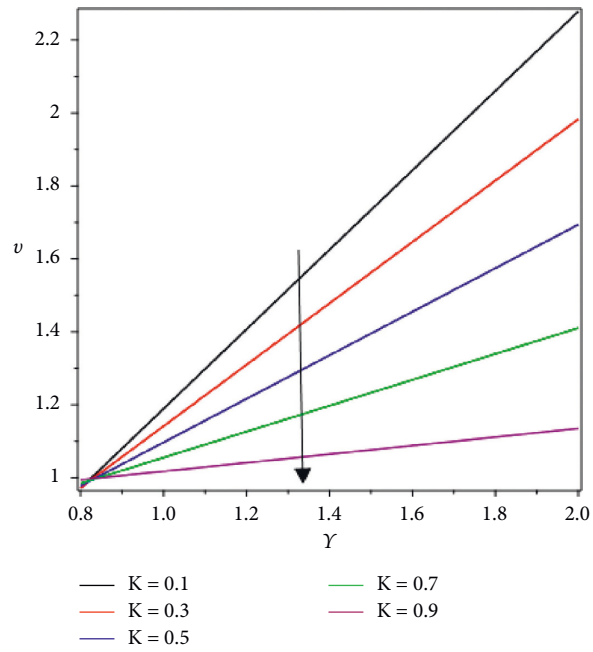

Figure 18: Impact of K on coating thickness.

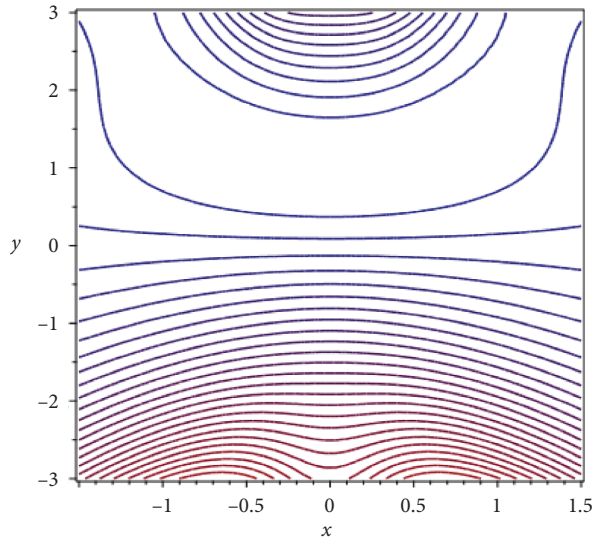

Figure 19: Streamline for $K = 0.1$ and $\lambda = 0.5446$ by fixing $\beta = 0.5$.

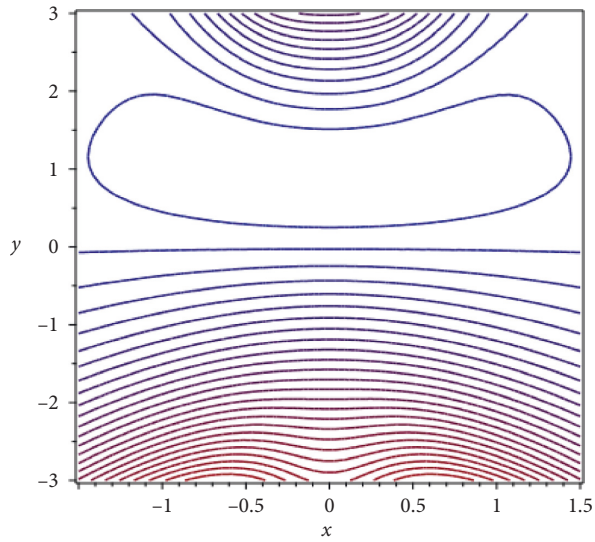

Figure 20: Streamline for $K = 0.3$ and $\lambda = 0.4207$ by fixing $\beta = 0.5$.

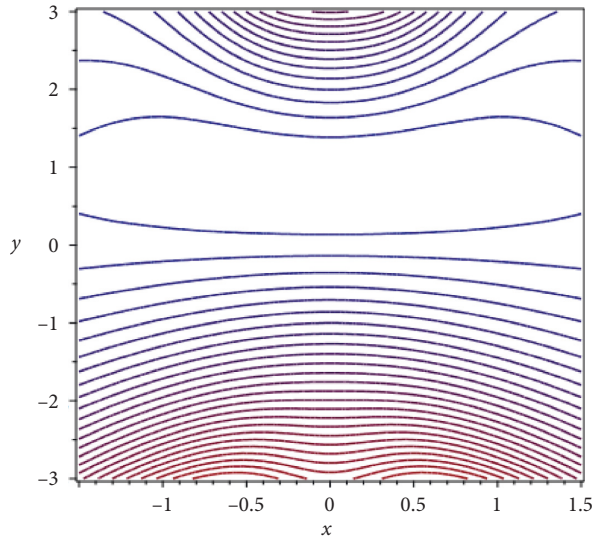

Figure 21: Streamline for $K = 0.5$ and $\lambda = 0.2984$ by fixing $\beta = 0.5$.

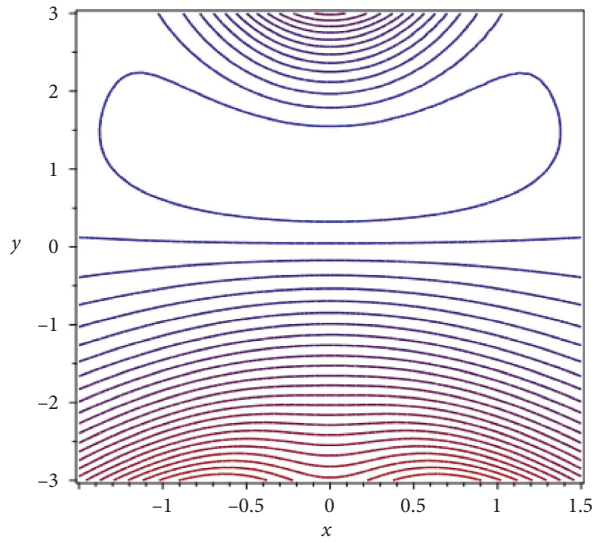

Figure 22: Streamline for $\beta = 0.1$ and $\lambda = 0.4889$ by fixing $K = 0.2$.

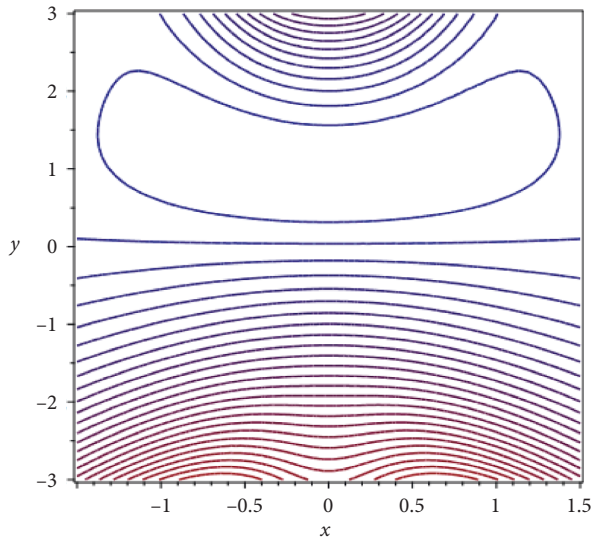

Figure 23: Streamline for $\beta = 0.3$ and $\lambda = 0.4856$ by fixing $K = 0.2$.

Figure 18 illustrates the graphical appearances of thickness of coating for various values of velocities K. One can observe that the existing coating thickness is declining function of K. Streamline pattern for fluid flow is sketched in Figures 19–23.

7. Conclusions

Reverse roll coating for a non-isothermal, incompressible third-grade fluid is theoretically evaluated. The perturbation approach is used to generate analytical solutions for the velocity profile, pressure gradients, and temperature distribution. In numerical form, the coating thickness, separation pointes, flow rate, power input, pressure distributions, and force of roll separation are tabularized.

The following are the main conclusions drawn from this study:

(i) The maximum coating thickness 1.0803 has been observed for $K = 0.1$, whereas the minimum thickness of the coating 1.0057 was found at $K = 0.9$.

(ii) The coating thickness to the highest can be as high as 1.0796 beside the separation point is 0.6620 for $\beta = 0.1$, whereas the minimum coating thickness 1.0573 has been observed for $\beta = 0.9$.

(iii) The magnitude of power input and roll separation force increases by rising the values of β.

(iv) The velocity of the flow and pressure gradients decreases as β increases.

(v) The peak velocity arises on the surface of reverse roll.

(vi) The absolute pressure gradient is at its highest point at the nip point.

(vii) Third-grade parameter plays important role to control the pressure gradients.

(viii) The pressure distributions increase as the third-grade parameter increases, while it decreases as the velocities ratio increase.

(ix) The temperature profiles are increasing function of K, β, and Υ.

(x) Third-grade parameter offers an economical device to regulator the velocity, coating thickness of the web, and flow rate.

(xi) If $\beta \longrightarrow 0$, the results of [35] are recovered.

Nomenclature

R: The radius of each roll
T: Extra stress tensor
ρ: Fluid density
K: Velocities ratio
C_p: Specific heat capacity
β: Non-Newtonian fluid parameter
Υ: Brickman number
H_0: Half of the nip separation
λ: Coating thickness
F: Dimensionless roll separation force
P: Modified pressure
θ: Temperature distribution.

Data Availability

The datasets supporting the conclusions of this article are included in the article.

Additional Points

In order to validate our findings in a real environment on an experimental basis, we invite scientists and engineers working in connected industries from all over the world. The theoretical investigation of viscoelastic materials was the primary focus of our research.

Conflicts of Interest

The authors declare that they have no conflicts of interest.

References

[1] H. U. Rasheed, S. Islam, and Z. Khan, "Computational analysis of hydromagnetic boundary layer stagnation point flow of nano liquid by a stretched heated surface with convective conditions and radiation effect," *Advances in Mechanical Engineering*, vol. 13, no. 10, 2021.

[2] Z. Zeeshan, "Second law and entropy generation analysis of magnetized viscous fluid flow over a permeable expandable sheet with nonlinear thermal radiation: brownian and thermophoresis effect," *Advances in Mechanical Engineering*, vol. 14, no. 1, 2022.

[3] H. U. Rasheed, A. A. Zubaidi, S. Islam, S. Saleem, Z. Khan, and W. Khan, "Effects of Joule heating and viscous dissipation on magnetohydrodynamic boundary layer flow of Jeffrey nanofluid over a vertically stretching cylinder," *Coatings*, vol. 11, no. 3, p. 353, 2021.

[4] S. Akram, M. Athar, K. Saeed, and A. Razia, "Impact of slip on nanomaterial peristaltic pumping of magneto-Williamson

nanofluid in an asymmetric channel under double-diffusivity convection," *Pramana*, vol. 96, no. 1, p. 57, 2022.

[5] S. M. Seyedhosseini, M. J. Esfahani, and M. Ghaffari, "A novel hybrid algorithm based on a harmony search and artificial bee colony for solving a portfolio optimization problem using a mean-semi variance approach," *Journal of Central South University*, vol. 23, no. 1, pp. 181–188, 2016.

[6] F. Arslan, "LMS algorithm for adaptive transversal equalization of a linear dispersive communication channel," *Review of Computer Engineering Research*, vol. 7, no. 2, pp. 73–85, 2020.

[7] A. B. W. Putra, "Computer technology simulation towards power generation potential from coproduced fluids in south lokichar oil fields," *International Journal of Communication and Computer Technologies*, vol. 8, no. 2, pp. 9–12, 2020.

[8] K. M. K. Rao, N. J. Aneela, K. Y. Sri, K. N. Prasanna, N. Sahithi, and L. Likhitha, "Design of clocked jk flip flop using air hole structured photonic crystal," *Journal of VLSI and Computer Systems*, vol. 3, no. 2, pp. 11–20, 2021.

[9] F. Gao, D. Yu, and Q. Sheng, "Analytical treatment of unsteady fluid flow of nonhomogeneous nanofluids among two infinite parallel surfaces: collocation method-based study," *Mathematics*, vol. 10, no. 9, p. 1556, 2022.

[10] D. Yu and R. Wang, "An optimal investigation of convective fluid flow suspended by carbon nanotubes and thermal radiation impact," *Mathematics*, vol. 10, no. 9, p. 1542, 2022.

[11] K. Wang, H. Wang, and S. Li, "Renewable quantile regression for streaming datasets," *Knowledge-Based Systems*, vol. 235, Article ID 107675, 2022.

[12] R. Fosdick and K. Rajagopal, "Thermodynamics and stability of fluids of third grade," *Proceedings of the Royal Society of London. A. Mathematical and Physical Sciences*, vol. 369, no. 1738, pp. 351–377, 1980.

[13] A. Zaib, A. J. Chamkha, M. M. Rashidi, and K. Bhattacharyya, "Impact of nanoparticles on flow of a special non-Newtonian third-grade fluid over a porous heated shrinking sheet with nonlinear radiation," *Nonlinear Engineering*, vol. 7, no. 2, pp. 103–111, 2018.

[14] F. Carapau, P. Correia, and L. M. Grilo, "Specific shear-dependent viscoelastic third-grade fluid model," in *Proceedings of the AIP Conference Proceedings*, vol. 1790, no. 1, AIP Publishing LLC, Melville, NY, U.S.A, December 2016.

[15] S. Akram, A. Razia, M. Y. Umair, T. Abdulrazzaq, and R. Z. Homod, "Double-diffusive convection on peristaltic flow of hyperbolic tangent nanofluid in non-uniform channel with induced magnetic field," *Mathematical Methods in the Applied Sciences*, 2022.

[16] M. Akram, U. Amjad, J. C. R. Alcantud et al., "Complex fermatean fuzzy N-soft sets: a new hybrid model with applications," *Journal of Ambient Intelligence and Humanized Computing*, pp. 1–34, 2022.

[17] M. Zahid, T. Haroon, M. Rana, and A. Siddiqui, "Roll coating analysis of a third grade fluid," *Journal of Plastic Film and Sheeting*, vol. 33, no. 1, pp. 72–91, 2017/01/01 2016.

[18] E. J. Hinch, *Perturbation Methods*, Cambridge University Press, Cambridge, NY, U.S.A, 1991.

[19] H. Friedrich and A. H. Nayfeh, *Introduction to perturbation techniques*, vol. 61, no. 12, p. 666, John Wiley & Sons, Hoboken, NJ, U.S.A, 1981.

[20] Z. Abbas and S. Khaliq, "Roll-over-web coating analysis of micropolar-Casson fluid: a theoretical investigation," *Journal of Polymer Engineering*, vol. 41, no. 4, pp. 289–298, 2021.

[21] F. Belblidia, H. R. T. Jahromi, S. O. S. Echendu, and M. F. Webster, "Reverse roll-coating flow: a computational investigation towards high-speed defect free coating," *Mechanics of Time-dependent Materials*, vol. 17, no. 4, pp. 557–579, 2013.

[22] F. Balzarotti and M. Rosen, "Systematic study of coating systems with two rotating rolls," *Latin American Applied Research*, vol. 39, pp. 99–104, 06/01 2009.

[23] I. Zeeshan, I. Khan, N. Amina, and N. N. Alshammari, "Double-layer coating using MHD flow of third-grade fluid with Hall current and heat source/sink," *Open Physics*, vol. 19, no. 1, pp. 683–692, 2021.

[24] S. Sofou and E. Mitsoulis, "Roll-over-web coating of pseudoplastic and viscoplastic sheets using the lubrication approximation," *Journal of Plastic Film and Sheeting*, vol. 21, no. 4, pp. 307–333, 2005.

[25] G. Zheng, F. Wachter, A. A. Zoubi et al., "Computations of coating windows for reverse roll coating of liquid films," *Journal of Coatings Technology and Research*, vol. 17, no. 4, pp. 897–910, 2020.

[26] H. Benkreira, M. F. Edwards, and W. L. Wilkinson, "A semi-empirical model of the forward roll coating flow of Newtonian fluids," *Chemical Engineering Science*, vol. 36, no. 2, pp. 423–427, 1981.

[27] Y. Hao and S. Haber, "Reverse roll coating flow," *International Journal for Numerical Methods in Fluids*, vol. 30, no. 6, pp. 635–652, 1999.

[28] S. Liu, X. He, F. T. S. Chan, and Z. Wang, "An extended multi-criteria group decision-making method with psychological factors and bidirectional influence relation for emergency medical supplier selection," *Expert Systems with Applications*, vol. 202, Article ID 117414, 2022.

[29] H. Benkreira, M. F. Edwards, and W. L. Wilkinson, "Roll coating of purely viscous liquids," *Chemical Engineering Science*, vol. 36, no. 2, pp. 429–434, 1981.

[30] J. Greener and S. Middleman, "Theoretical and experimental studies of the fluid dynamics of a two-roll coater," *Industrial & Engineering Chemistry Fundamentals*, vol. 18, no. 1, pp. 35–41, 1979.

[31] M. Decré, E. Gailly, and J. M. Buchlin, "Meniscus shape experiments in forward roll coating," *Physics of Fluids*, vol. 7, no. 3, pp. 458–467, 1995.

[32] R. Mücke, O. Büchler, M. Bram, A. Leonide, E. I. Tiffée, and H. P. Buchkremer, "Preparation of functional layers for anode-supported solid oxide fuel cells by the reverse roll coating process," *Journal of Power Sources*, vol. 196, no. 22, pp. 9528–9535, 2011.

[33] S. Alonso, F. Bertrand, and P. A. Tanguy, "A torque-based analysis of the reverse roll coating process," *Chemical Engineering Science*, vol. 58, no. 9, pp. 1831–1837, 2003.

[34] E. Pitts and J. Greiller, "The flow of thin liquid films between rollers," *Journal of Fluid Mechanics*, vol. 11, no. 1, pp. 33–50, 2006.

[35] J. Greener and S. Middleman, "Reverse roll coating of viscous and viscoelastic liquids," *Industrial & Engineering Chemistry Fundamentals*, vol. 20, no. 1, pp. 63–66, 1981.

[36] W. S. Ho and F. A. Holland, "between-rolls metering coating technique," *A Theoretical and Experimental Study*, vol. 61, 1978.

[37] J. Taylor and A. Zettlemoyer, "Hypothesis on the mechanism of ink splitting during printing," *Tappi Journal*, vol. 12, pp. 749–757, 1958.

[38] J. Hintermaier and R. White, "The splitting of a water film between rotating rolls," *Tappi Journal*, vol. 48, pp. 617–625, 1965.

[39] F. Ali, Y. Hou, M. Zahid, and M. A. Rana, "Theoretical study of the reverse roll coating of non-isothermal magnetohydrodynamics viscoplastic fluid," *Coatings*, vol. 10, no. 10, p. 940, 2020.

[40] F. Ali, Y. Hou, M. Zahid, and M. Rana, "Mathematical analysis of pseudoplastic polymers during reverse roll-coating," *Polymers*, vol. 12, no. 10, p. 2285, 2020.

[41] M. Zahid, I. Siddique, S. Saleem, A. Al-Zubaidi, M. A. Rana, and M. Zafar, "Forward roll coating of a williamson's material onto a moving web: a theoretical study," *Mathematical Problems in Engineering*, vol. 2021, Article ID 3431885, pp. 1–11, 2021.

[42] M. Zafar, M. A. Rana, M. Zahid, and B. Ahmad, "Mathematical analysis of the coating process over a porous web lubricated with upper-convected maxwell fluid," *Coatings*, vol. 9, no. 7, p. 458, 2019.

[43] L. Cai, L. Xiong, J. Cao, H. Zhang, and F. E. Alsaadi, "State Quantized Sampled-Data Control Design for Complex-Valued Memristive Neural Networks," *Journal of the Franklin Institute*, 2022.

[44] G. Xiao, B. Chen, S. Li, and X. Zhuo, "Fatigue life analysis of aero-engine blades for abrasive belt grinding considering residual stress," *Engineering Failure Analysis*, vol. 131, Article ID 105846, 2022.

[45] Y. Wang, H. Wang, B. Zhou, and H. Fu, "Multi-dimensional prediction method based on Bi-LSTMC for ship roll," *Ocean Engineering*, vol. 242, Article ID 110106, 2021.

[46] F. Ning, G. He, C. Sheng et al., "Yarn on yarn abrasion performance of high modulus polyethylene fiber improved by graphene/polyurethane composites coating," *Journal of Engineered Fibers and Fabrics*, vol. 16, 2021.

[47] C. Sheng, G. He, Z. Hu et al., "Yarn on yarn abrasion failure mechanism of ultrahigh molecular weight polyethylene fiber," *Journal of Engineered Fibers and Fabrics*, vol. 16, 2021.

[48] M. Ayub, A. Rasheed, and T. Hayat, "Exact flow of a third grade fluid past a porous plate using homotopy analysis method," *International Journal of Engineering Science*, vol. 41, no. 18, pp. 2091–2103, 2003.

[49] A. M. Siddiqui, R. Mahmood, and Q. K. Ghori, "Thin film flow of a third grade fluid on a moving belt by He's homotopy perturbation method," *International Journal of Nonlinear Sciences and Numerical Stimulation*, vol. 7, no. 1, pp. 7–14, 2006.

[50] A. M. Siddiqui, M. Hameed, B. M. Siddiqui, and Q. K. Ghori, "Use of Adomian decomposition method in the study of parallel plate flow of a third grade fluid," *Communications in Nonlinear Science and Numerical Simulation*, vol. 15, no. 9, pp. 2388–2399, 2010.

[51] A. M. Siddiqui, M. Zahid, M. A. Rana, and T. Haroon, "Calendering analysis of a non-Newtonian material," *Springer Proceedings in Mathematics & Statistics," in Advances in Applied Mathematics*, pp. 179–196, Springer, Berlin, Germany, 2014.

[52] D. J. Coyle, C. W. Macosko, and L. E. Scriven, "The fluid dynamics of reverse roll coating," *AIChE Journal*, vol. 36, no. 2, pp. 161–174, 1990.